OI: 10.3901/CJME.2013.01.095, available online at www.springerlink.com; www.cjmenet.com; www.cjmenet.com.cn

Unbalance Vibratory Displacement Compensation for Active Magnetic Bearings

GAO Hui*, XU Longxiang, and ZHU Yili

College of Mechanical and Electrical Engineering, Nanjing University of Aeronautics and Astronautics, Nanjing 210016, China

Received March 10, 2012; revised August 2, 2012; accepted September 12, 2012

Abstract: As the dynamic stiffness of radial magnetic bearings is not big enough, when the rotor spins at high speed, unbalance displacement vibration phenomenon will be produced. The most effective way for reducing the displacement vibration is to enhance the radial magnetic bearing stiffness through increasing the control currents, but the suitable control currents are not easy to be provided, especially, to be provided in real time. To implement real time unbalance displacement vibration compensation, through analyzing active magnetic bearings (AMB) mathematical model, the existence of radial displacement runout is demonstrated. To restrain the runout, a new control scheme-adaptive iterative learning control (AILC) is proposed in view of rotor frequency periodic uncertainties during the startup process. The previous error signal is added into AILC learning law to enhance the convergence speed, and an impacting factor β influenced by the rotor rotating frequency is introduced as learning output coefficient to improve the rotor control effects. As a feed-forward compensation controller, AILC can provide one unknown and perfect compensatory signal to make the rotor rotate around its geometric axis through power amplifier and radial magnetic bearings. To improve AMB closed-loop control system robust stability, one kind of incomplete differential PID feedback controller is adopted. The correctness of the AILC algorithm is validated by the simulation of AMB mathematical model adding AILC compensation algorithm through MATLAB soft. And the compensation for fixed rotational frequency is implemented in the actual AMB system. The simulation and experiment results show that the compensation scheme based on AILC algorithm as feed-forward compensation and PID algorithm as close-loop control can realize AMB system displacement minimum compensation at one fixed frequency, and improve the stability of the control system. The proposed research provides a new adaptive iterative learning control algorithm and control strategy for AMB displacement minimum compensation, and provides some references for time-varied displacement minimum compensation.

Key words: active magnetic bearings, unbalance displacement compensation, mathematical model, adaptive iterative learning control

1 Introduction

As emerging products and rotating machinery, active magnetic bearings (AMB) have been moved from promising concepts to practical application. It has some advantages over conventional bearings, which are exhibited as follows: contact-free support, higher speeds, and active control[1]. However, unbalance response synchronous with rotor frequency is existent because of mass unbalance and asymmetry, which would generate force vibrations and displacement vibrations. For unbalance displacement vibrations, corresponding compensation schemes have been adopted from the 1990s[2–13]. The schemes purposes are to make the rotors rotate around there geometry axes to reduce rotors radial runout.

JING, et al[2], restricted the unbalance force utilizing one external, and suitable force injected into the AMB system. HU, et al[3], achieved prior the unbalance force and couples through holographical spectral analysis, then calculated the unbalance compensatory currents and injected them into the control currents. Overseas, TAGUCHI, et al[4], proposed a vibration control system using active magnetic bearings to cope with a sudden sinusoidal disturbance. A new approach called adaptive auto-centering approach was presented in Ref. [5], which can perform on-line identification of rotor imbalance and compensate for transmitted force. MIZUNO, et al[6], presented a method for unbalance compensation in AMB to achieve displacement, current, or force regulation, the key of it was pole-zero cancellation compensation. NONAMI, et al[7], focused on the error of estimated frequency of disturbance and presented a new adaptive frequency tracking and new modified law, then added a corresponding signal in the original control system. ARIAS, et al[8], presented a LQR scheme for vibration control in a rotor system to reduce the vibrations caused by the rotor imbalance in the two disks using only an actuator. The compensation of the active magnetic bearing actuator nonlinearities was demonstrated in Ref. [9] for a variable force bias control. INOUE, et al[10],

* Corresponding author. E-mail: gaohui2010@nuaa.edu.cn
This project is supported by National Natural Science Foundation of China (Grant No. 50437010), National Hi-tech Research and Development Program of China (863 Program, Grant No. 2006AA05Z205), and Fund of Aeronautics Science of China (Grant No. 2008ZB52018)

proposed a vibration control method for rotor systems utilizing disturbance observer. Moreover, the application of iterative learning control (ILC) was analyzed in the unbalance compensation for AMB system in Refs. [11–13], and achieved simulations[11] or experiments[12–13]. Various methods have been discussed and most of them can achieve satisfying control effects. However, most of the existent compensatory methods require AMB precise information or cannot achieve online displacement compensation, which limit the application of these approaches.

In this paper, the AMB mathematical model is established and rotor system unbalance response is analyzed, the response can increase rotor radial runout. To restrain the runout, an adaptive ILC (AILC) algorithm is proposed as a feed-forward compensation controller (FFC). To improve the learning convergence speed, the error signal of previous control circle is used in the control output, and to reduce the learning effects in uncompensated frequency range, a novel impacting factor β as learning output coefficient is introduced. The role of β is to weaken ILC influence for AMB control system in the process from static state suspension to one given frequency. And the AILC can provide some desired and unknown signals to restrict the rotor to rotate around its geometrical axis by means of the radial magnetic bearings. Then the unbalance displacement compensation could be implemented.

2 AMB Radial Model and Displacement Vibration Analysis

2.1 One DOF control subsystem

To have verisimilar effects in radial four degree-of-freedoms (DOFs) mathematical model and the later simulation, this section firstly analyzes one DOF subsystem control principle because the decentralized control is adopted during the experiment. For simplicity, the analysis is only done in the *X*-direction and all the coupling effects among the different axes and non-collocation are ignored. Fig. 1 shows the control structure of one DOF subsystem of radial magnetic bearings.

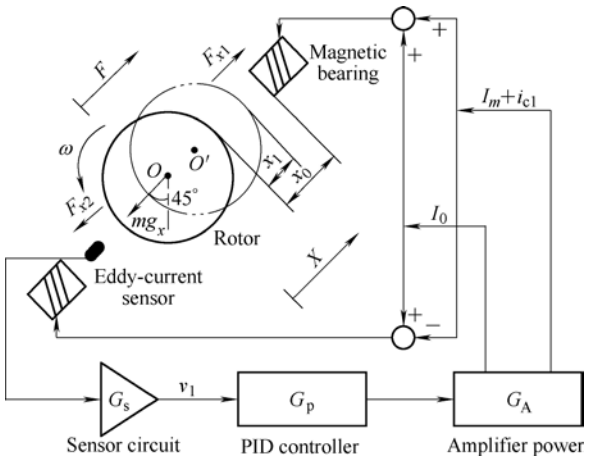

Fig. 1. Structure of a one-DOF AMB system

When the rotor is static stable suspense, the electromagnetic force influencing on the rotor can be written as

$$F_{x0}=\frac{\mu_0 AN^2}{4}\left[\left(\frac{I_0+I_m}{x_0}\right)^2-\left(\frac{I_0-I_m}{x_0}\right)^2\right]=mg_x, \quad (1)$$

where the parameters of Eq. (1) is given in Table 1. The gravity of the rotor is based on the static feedback current I_m. Here, I_m=0.1 A. If the rotor rotates and the compensation control is not added, the electromagnetic force is expressed by

$$F_x=F_{x1}-F_{x1}=\frac{\mu_0 AN^2}{4}\times \left[\left(\frac{I_0+I_m+i_{c1}}{x_0-x_1}\right)^2-\left(\frac{I_0-I_m-i_{c1}}{x_0+x_1}\right)^2\right], \quad (2)$$

where x_1 is the radial vibratory displacement and i_{c1} is the control current. The Taylor Series of Eq. (2) at the point (x_1, i_{c1}), where x_1 and i_{c1} are zeros, can be written as

$$F_{x\left|\begin{matrix}x_1=0\\ i_{c1}=0\end{matrix}\right.}=F_{x0}+K_{x1}x_1+K_{i1}i_{c1}+\mu_0 AN^2\frac{I_m}{x_0^3}x_1 i_{c1}+\cdots \quad (3)$$

where $K_{x1}=\mu_0 AN^2\cdot(I_0^2+I_m^2)/x_0^3$ is the displacement stiffness, and $K_{i1}=\mu_0 AN^2 I_0/x_0^2$ is the current stiffness, their values are given in Table 1. $\mu_0 AN^2 I_m x_1 i_{c1}/x_0^3+\cdots$ is an infinitesimal of higher order or nonlinear small, therefore, it can be ignored. Therefore, Eq. (3) can be replaced by

$$\Delta F_x=K_{x1}x_1+K_{i1}i_{c1}, \quad (4)$$

where ΔF_x is the linear and dynamic resultant force.

Table 1. Parameters of AMB system

Parameter	Value
Air permeability μ_0/(μV • s • (A • m)$^{-1}$)	0.4π
Pole area A/cm^2	2.79
Numbers of the coils N	130
Gap of the rotor at balance position x_0/mm	0.25
Gravity acceleration in X axis and Y axis g_x, g_y/(m • s^{-2})	6.93
Bias current I_0/A	2
Mass of the rotor m/kg	2.8
Transverse moments of inertia I_r/(kg • m^2)	0.021 4
Polar moments of inertia I_a/(g • m^2)	0.764 6
Distance of left AMB l_1/m	0.120 2
Distance of right AMB l_2/m	0.133 8
Sum distance of l_1 and l_2 l/m	0.254
Stiffness coefficient for displacement k_{xn}/(MN • m^{-1})	1.517
Stiffness coefficient for current k_{in}/(N • A^{-1})	189.6
Linear amplifier power gain G_a/(A • V^{-1})	0.4
Linear sensor gain G_s/(kV • m^{-1})	20

In Table 1, n=1, 2, 3, 4. According to Fig. 1 and Table 1, the relationship between x_1 and i_{c1} is deduced:

$$i_{c1} = x_1 G_s G_p G_a = -8\,000 x_1 G_p, \tag{5}$$

where

$$G_p(s) = K_p\left(1+\frac{1}{T_i s}+\frac{T_d s}{1+T_f s}\right). \tag{6}$$

Eq. (6) is a digital PID controller with incomplete derivation. where K_p is the proportional gain, T_i is the integral gain, T_d is differential gain, and $T_d/(1+T_f)$ is the incomplete differential part. The frequency characteristic of Eq. (6) can be achieved:

$$G_p(j\omega) = G_p(s)\big|_{s=j\omega}. \tag{7}$$

According to Eqs. (4)–(7), the resultant force is mainly influenced by the radial displacement x_1 and the gain of PID controller, and it can provide basis for the design and analysis of four radial DOFs subsystems mathematical model.

2.2 Modeling of four radial subsystems for AMB

To synthetically analyze the generating mechanism of AMB radial runout and verify the feasibility and effectiveness of compensation scheme, the mathematical model of AMB four radial subsystems is established.

For the thrust force in the rotor axial can be assumed passing through the mass center of the rotor, and the rotor does not exist unbalance in axial direction, the axial subsystem can be separated from the other four radial DOFs. And the rotor force analysis in the four radial directions is shown in Fig. 2. Where, O_g is the mass center and O_c is the geometric center; and each electromagnet force is defined as F_n ($n = x_{jk}$ or y_{jk}, j = 1, 2 and k = 1, 2).

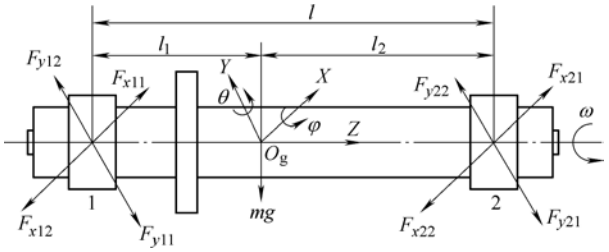

Fig. 2. Stress analysis for the radial rotor subsystems

According to the motion theorem of the mass centre, the dynamic model of the AMB rotor is described by the equations as follows[14–15]:

$$\begin{cases} m\ddot{x}_g = F_{x11} - F_{x12} + F_{x21} - F_{x22} - mg_x - f_x, \\ m\ddot{y}_g = F_{y11} - F_{y12} + F_{y21} - F_{y22} - mg_y - f_y, \\ I_r\ddot{\phi} - \omega I_a\dot{\theta} = (F_{y11} - F_{y12})\cdot l_1 - (F_{y21} - F_{y22})\cdot l_2, \\ I_r\ddot{\theta} + \omega I_a\dot{\phi} = -(F_{x11} - F_{x12})\cdot l_1 + (F_{x21} - F_{x22})\cdot l_2, \end{cases} \tag{8}$$

where

$$\begin{cases} f_x = me_r\omega^2\cos(\omega t+\phi), \\ f_y = me_r\omega^2\sin(\omega t+\phi). \end{cases} \tag{9}$$

Eq. (9) are the inertia force in the x and y directions, e_r is the distance between the mass center and the rotational center (in Fig. 3), and ω is the rotor rotational angular velocity. Due to the relatively smaller magnetic bearing stiffness, the rotor would rotate around an unknown axis between the principal axis of inertia and its geometric axis. For the rotor can be considered as a rigid body[14], its eccentric position in mass center section is shown in Fig. 3.

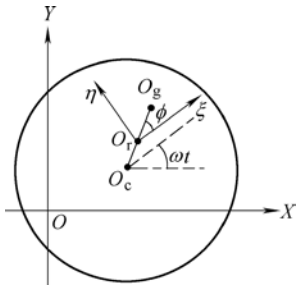

Fig. 3. Rotor eccentric position

where $\overline{O_r O_g} = e_r$, $\overline{O_c O_g} = e$ is the eccentricity, OXY coordinate system is fixed on the radial magnetic bearings center and $O_r\xi\eta$ is the rotor rotating coordinate system. Geometric center movement is the key to analyze rotor trajectories but not mass center movement, and the relationship between mass center and geometric center is calculated

$$\begin{cases} x_g = x_c + e\cos(\omega t+\phi), \\ y_g = y_c + e\sin(\omega t+\phi), \end{cases} \tag{10}$$

where x_c and y_c are the coordinate value of the geometric center.

The vibration mechanical model in matrix form of the four radial subsystems is established by means of Eqs. (8)–(10) and the Refs. [1, 16–17], which is shown as follows:

$$\begin{pmatrix} \frac{l_2}{l}m & \frac{l_1}{l}m & 0 & 0 \\ 0 & 0 & \frac{l_2}{l}m & \frac{l_1}{l}m \\ 0 & 0 & -\frac{I_r}{l} & \frac{I_r}{l} \\ -\frac{I_r}{l} & \frac{I_r}{l} & 0 & 0 \end{pmatrix} \begin{pmatrix} \ddot{x}_1 \\ \ddot{x}_2 \\ \ddot{y}_1 \\ \ddot{y}_2 \end{pmatrix} + \begin{pmatrix} 0 & 0 & 0 & 0 \\ 0 & 0 & 0 & 0 \\ \frac{\omega I_a}{l} & -\frac{\omega I_a}{l} & 0 & 0 \\ 0 & 0 & -\frac{\omega I_a}{l} & \frac{\omega I_a}{l} \end{pmatrix} \times$$

$$\begin{pmatrix} \dot{x}_1 \\ \dot{x}_2 \\ \dot{y}_1 \\ \dot{y}_2 \end{pmatrix} = \begin{pmatrix} k_{x1} & k_{x2} & 0 & 0 \\ 0 & 0 & k_{x3} & k_{x4} \\ 0 & 0 & l_1 k_{x3} & -l_2 k_{x4} \\ -l_1 k_{x1} & l_2 k_{x2} & 0 & 0 \end{pmatrix} \begin{pmatrix} x_1 \\ x_2 \\ y_1 \\ y_2 \end{pmatrix} +$$

$$\begin{pmatrix} k_{i1} & k_{i2} & 0 & 0 \\ 0 & 0 & k_{i3} & k_{i4} \\ 0 & 0 & l_1 k_{i3} & -l_2 k_{i4} \\ -l_1 k_{i1} & l_2 k_{i2} & 0 & 0 \end{pmatrix} \begin{pmatrix} i_{c1} \\ i_{c2} \\ i_{c3} \\ i_{c4} \end{pmatrix} + \begin{pmatrix} 1 & 0 & 0 & 0 \\ 0 & 1 & 0 & 0 \\ 0 & 0 & 0 & 0 \\ 0 & 0 & 0 & 0 \end{pmatrix} \begin{pmatrix} f_x' \\ f_y' \\ 0 \\ 0 \end{pmatrix}, \quad (11)$$

where

$$\begin{cases} f_x' = m(e-e_r)\omega^2 \cos(\omega t+\phi), \\ f_y' = m(e-e_r)\omega^2 \sin(\omega t+\phi), \end{cases} \quad (12)$$

$$\begin{cases} x_c = \dfrac{l_2 x_1 + l_1 x_2}{l}, \\ y_c = \dfrac{l_2 y_1 + l_1 y_2}{l}, \\ \theta = \dfrac{y_2 - y_1}{l}, \\ \phi = \dfrac{x_2 - x_1}{l}. \end{cases} \quad (13)$$

The values and meanings of l_1, l_2, l, I_a and I_r, and so on, are given in Table 1.

2.3 Vibration displacement analysis

Eq. (11) can be expressed as

$$\boldsymbol{M}\ddot{\bar{\boldsymbol{x}}} + \boldsymbol{C}\dot{\bar{\boldsymbol{x}}} + \boldsymbol{K}\bar{\boldsymbol{x}} = \boldsymbol{B}\bar{\boldsymbol{i}}_c + \boldsymbol{E}\bar{\boldsymbol{f}}', \quad (14)$$

where $\bar{\boldsymbol{x}} = [x_1, x_2, y_1, y_2]^T$ is the displacement vector, $\bar{\boldsymbol{i}}_c = [i_{c1}, i_{c2}, i_{c3}, i_{c4}]^T$ is the control current vector, and $\bar{\boldsymbol{f}}' = [f_x', f_y', 0, 0]^T$ is the harmonic disturbance forces vector. $\boldsymbol{M}$ is the mass matrix, $\boldsymbol{C}$ is the damping matrix, $\boldsymbol{K}$ is the displacement stiffness matrix, $\boldsymbol{B}$ is the current stiffness matrix, and $\boldsymbol{E}$ is disturbance force coefficient matrix.

According to Eqs. (5)–(7), the matrix equations Eq. (14) can be transformed as

$$\boldsymbol{M}\ddot{\bar{\boldsymbol{x}}} + \boldsymbol{C}\dot{\bar{\boldsymbol{x}}} + \boldsymbol{K}'\bar{\boldsymbol{x}} = \boldsymbol{E}\bar{\boldsymbol{f}}, \quad (15)$$

where

$$\boldsymbol{K}' = \boldsymbol{K} + 8\,000 G_p(j\omega)\cdot\boldsymbol{B}. \quad (16)$$

Eq. (16) is the AMB generalized dynamic stiffness which can influence rotor system moving trajectories. Moreover, Eq. (16) is accord with damp system forced vibration in harmonic force action, and it can be rewritten as[14]

$$\ddot{\bar{\boldsymbol{x}}} + 2\boldsymbol{\zeta}\boldsymbol{\omega}_n\dot{\bar{\boldsymbol{x}}} + \boldsymbol{\omega}_n^2\bar{\boldsymbol{x}} = \boldsymbol{M}^{-1}\boldsymbol{E}\bar{\boldsymbol{f}}', \quad (17)$$

where

$$\boldsymbol{\omega}_n^2 = \boldsymbol{M}^{-1}\boldsymbol{K}', \ \boldsymbol{\zeta} = \frac{\boldsymbol{M}^{-1}\boldsymbol{C}}{2\boldsymbol{\omega}_n}. \quad (18)$$

$\boldsymbol{\omega}_n$ is ABM natural frequency matrix, and $\boldsymbol{\zeta}$ is its relative damping coefficient matrix. The solution of Eq. (17) can be given as

$$\bar{x}(t) = [a\exp(-\boldsymbol{\zeta}\boldsymbol{\omega}_n t)\sin(\boldsymbol{\omega}_n t) + B_d \sin(\omega t + \psi_d)]\boldsymbol{T}, \quad (19)$$

where

$$\tilde{\bar{u}}(t) = a\exp(-\boldsymbol{\zeta}\boldsymbol{\omega}_n t)\sin(\boldsymbol{\omega}_n t)\boldsymbol{T}, \quad (20)$$

$$\bar{u}^*(t) = B_d \sin(\omega t + \psi_d)\boldsymbol{T}, \quad (21)$$

$$B_d = \frac{\boldsymbol{\omega}_n^2 m(e-e_r)\omega^2}{\boldsymbol{K}'[(\boldsymbol{\omega}_n^2 - \omega^2)^2 + 2\boldsymbol{\zeta}\boldsymbol{\omega}_n\omega]^{1/2}}. \quad (22)$$

In Eqs. (19)–(22), $\boldsymbol{T} = [1, 1, 1, 1]^T$, $\tilde{\bar{u}}(t)$ is the free vibration, $\bar{u}^*(t)$ is harmonic forced vibration, and B_d is $\bar{u}^*(t)$ amplitude. Because of the relatively smaller values of a and $\boldsymbol{\zeta}$ in the practical AMB system, $\tilde{\bar{u}}(t)$ effects for the whole system is weaker than $\bar{u}^*(t)$, in other words, the vibration displacement amplitude is mainly caused by $\bar{u}^*(t)$.

To test the effects of $\bar{u}^*(t)$ for system vibration, rotor geometric center orbit and one radial DOF displacement curve are simulated by programming of Eq. (11). The solutions of Eq. (11) are the rotational displacements of the rotor at radial magnetic bearings. The AMB parameters in Eq. (11) are given in Table 1, and PID controller parameters are given referring to experimental PID controller: K_p=0.585, T_i=0.545, T_d=0.619, T_f=0.753 9. Here, the rotational angular velocity ω is assumed to be 6 280 rad/s (200 Hz) because the unbalance vibratory displacement compensation will be implemented at 200 Hz, and the eccentricity e is assumed to be 15 μm. The rotor unbalance trajectory at radial MB is given in Fig. 4.

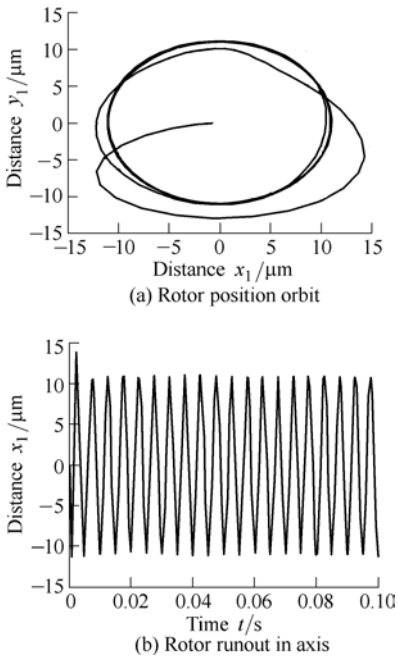

Fig. 4. Rotor unbalance trajectory at radial MB

The rotor radial vibration displacement (runout) exists in Fig. 4(b), and the vibration frequency coincides with the rotational frequency 200 Hz. The simulation result verifies the correctness of the analysis about Eqs. (19)–(22).

To concretely analyze the influence of harmonic forced vibration on the system, the transformation of Eq. (22) is

$$B_d = \frac{\boldsymbol{M}^{-1} m(e - e_r)\omega^2}{\boldsymbol{K}'[(\boldsymbol{M}^{-1}\boldsymbol{C} - \omega^2)^2 + 2\boldsymbol{M}^{-1}\boldsymbol{C}\omega]^{1/2}}. \tag{23}$$

In the vibration, amplitude B_d, $\boldsymbol{M}$, m, $\boldsymbol{C}$, e_r, and so on are depends only on the AMB rotor mechanical structure. Once the rotor structure has been designed, those parameters would be basically unchanged. The value of B_d is mainly affected by the generalized dynamic stiffness $\boldsymbol{K}'$ and the rotational angular frequency ω, so, to reduce rotor radial displacement vibration in a fixed frequency ω, the stiffness $\boldsymbol{K}'$ should be increased through increasing control current amplitudes according to Eqs. (5), (14), (16), and (23).

In the following, methods to increase the $\boldsymbol{K}'$ in Eq. (16) are analyzed. Because the displacement stiffness $\boldsymbol{K}$ and the current stiffness $\boldsymbol{B}$ are constant values in the AMB system, the PID controller becomes the most important part to increase the stiffness $\boldsymbol{K}'$. Therefore, the unbalance vibratory displacement compensation could be achieved through increasing the output gain of the controller by some control and compensation algorithms.

3 Adaptive Iterative Learning Control Scheme as Feed-forward Controller

3.1 Adaptive iterative learning controller

The ILC algorithm as a controller with memory function is widely applied in robots or manipulators to eliminate periodic tracking error[18–20]. The basic principle of ILC is to amend the control effects of the present cycle by learning the error information and the stored control information of past control cycle, and obtain perfect and unknown control signal. Refs. [11–13] all adopt ILC algorithms to compensate rotor unbalance vibratory displacement, however, Refs. [11–12] do not consider the periodic uncertainties of rotor rotational frequency. Ref. [13] proposes one compensation algorithm called ALC and it could change the learning cycle according to rotational speed vibration, but, in ALC application, the learning gains for a set of speed points must be obtained beforehand and the speed points should be distributed in the required speed range, which maybe affect ALC application in other AMB systems. Furthermore, Refs. [11–13] all did not analyze the influence of ILC algorithms on AMB unbalance compensation in the startup process of the rotor system.

In the running process of AMB rotor, it takes some time from static suspension to attain one fixed rotational speed. During the process, the speed is variable but ILC algorithms learning cycle is fixed, which makes previous learning gains be improperly added into the next control cycle. Large gain control errors can increase vibration and even make the whole system fail. To solve this problem, an adaptive ILC (AILC) algorithm serving as the feed-forward controller to implement vibratory displacement compensation is presented in Fig. 5. The control scheme consists of PID feedback control system, AILC feed-forward compensation controller and generalized plant. The PID controller can steady the whole system and improve the anti-interference ability, and the action of AILC is to make the learning gain accurately track the expectant orbit. The generalized plant includes power amplifier, electromagnetic coils, and rotor system.

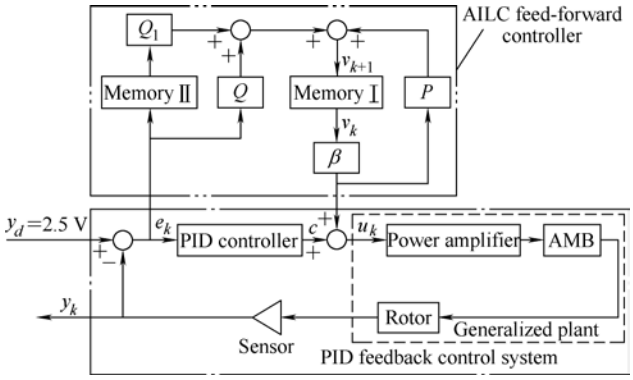

Fig. 5. AILC compensation principle of AMB system

To improve control performance and enhance the convergence rate of the learning law, there are two modifications in AILC. The first one is enhancing the error information action of previous control period, and the second one is proposing a novel impacting factor β as the coefficient of the learning v_k. β can reduce the effects of learning gain to the control system when rotor speed is not coincide with the learning cycle of AILC. AILC can implement vibratory displacement compensation without any information of the generalized plant, and it will not increase the interference of the feedback controller. Only the expectant signal y_d and the output of the sensor y_k are needed in AILC, here, y_d is 2.5 V witch is defined as the balance position of rotor during static suspension. The error signal between y_d and y_k is iteratively learned, then, the perfect and unknown control signal u_k is obtained as the input signal of the power amplifier.

The functions of AILC can be introduced by the iterative formulas in discrete domain. The error formula is given as

$$e_k(n) = y_d(n) - y_k(n),\ n \in \left[0, \frac{f_s}{f} - 1\right],\ n \in \{Z\}, \tag{24}$$

where n is the sampling points, f_s is the sampling frequency, f is the rotary frequency of the rotor, Z is the aggregate of all integers, and k is repetitive learning number.

The update learning law of AILC is summarized as

$$v_{k+1}(n) = \beta P v_k(n) + Q e_k(n) + Q_1 e_k(n-1). \tag{25}$$

The learning law of original ILC (OILC) in Ref. [18]

was given as

$$v_{k+1}(n) = v_k(n) + Qe_k(n). \tag{26}$$

Where in Eqs. (25) and (26), P, Q and Q_1 are the linear operators to improve the control performance of ILC algorithms, which should be determined by experiment debugging. Here, $e_k(n-1)$ and Q_1 are added into Eq. (25) as the modified link, so as to enhance the learning convergence rate by more utilizing the control error information, and the action of β is to implement adaptive compensation.

To understand the action of AILC better, the control input signal of generalized plant is written as

$$u_k(n) = c(n) + \beta v_k(n), \tag{27}$$

where $u_k(n)$ is the controller input, $c(n)$ is PID controller output, $v_k(n)$ is the learning gain of AILC, and β is the impacting factor of $v_k(n)$. The last objective is to obtain perfect controller signal u_d when having infinitely iterative learning, then make the error signal become zero. It should be satisfied as

$$\lim_{k\to\infty} u_k(n) = u_d,\ \lim_{k\to\infty} e_k(n) = 0. \tag{28}$$

3.2 Convergence analysis

The convergence of relational expressions of Eq. (28) will be proved when adding PID feedback controller in Fig. 5. The discrete transfer function of the learning law of Eq. (25) can be calculated by

$$V_{k+1}(z) = \beta P V_k(z) + QE_k(z) + Q_1 E_k(z)z^{-1} = \beta P V_k(z) + (Q + Q_1 z^{-1})E_k(z), \tag{29}$$

where z^{-1} represents the lag operator in time domain, and it could make the sampled signal lag one period. This is the reason why the former error information is added into the modified learning law of AILC.

The PID controller with incomplete differential part is given in time domain according to Eq. (6):

$$c(t) = G_{\mathrm{p}}(t) = K_{\mathrm{p}}\left[e(t) + \frac{1}{T_{\mathrm{i}}}\int_0^t e(t)\mathrm{d}t + \frac{T_{\mathrm{d}}}{1+T_{\mathrm{f}}}\frac{\mathrm{d}(e(t))}{\mathrm{d}t}\right]. \tag{30}$$

The difference equation of Eq. (30) can be calculated by

$$c(n) = K_{\mathrm{p}}\left[e(n) + \frac{1}{T_{\mathrm{i}}}\sum_{i=0}^{n} T_0 e(n-i) + \frac{T_{\mathrm{d}}}{1+T_{\mathrm{f}}}\frac{e(n)-e(n-1)}{T_0}\right]. \tag{31}$$

The discrete function of Eq. (30) is deduced as

$$C(z) = K_{\mathrm{p}}\left[1 + \frac{T_0}{T_{\mathrm{i}}}\frac{1}{1-z^{-1}} + \frac{T_{\mathrm{d}}}{(1+T_{\mathrm{f}})T_0}(1-z^{-1})\right]E(z). \tag{32}$$

The z-transform of the control signal function of Eq. (27) is deduced by

$$U_k(z) = C(z) + \beta V_k(z) = k_{\mathrm{p}}\left[1 + \frac{T_0}{T_{\mathrm{i}}}\frac{1}{1-z^{-1}} + \frac{T_{\mathrm{d}}}{(1+T_{\mathrm{f}})T_0}(1-z^{-1})\right]E(z) + \beta V_k(z). \tag{33}$$

Here, assuming

$$H(z) = \frac{1}{k_{\mathrm{p}}\left[1 + \frac{T_0}{T_{\mathrm{i}}}\frac{1}{1-z^{-1}} + \frac{T_{\mathrm{d}}}{(1+T_{\mathrm{f}})T_0}(1-z^{-1})\right]}. \tag{34}$$

The discrete function of error signal can be obtained as

$$E(z) = (U_k(z) - \beta V_k(z))H(z). \tag{35}$$

Putting Eq. (35) into Eq. (29), we can obtain

$$V_{k+1}(z) = \beta P V_k(z) + (Q + Q_1 z^{-1})(U_k(z) - \beta V_k(z)) \times H(z) = \beta[P - (Q + Q_1 z^{-1})H(z)]V_k(z) + (Q + Q_1 z^{-1})H(z)U_k(z). \tag{36}$$

Eq. (37) gives the transformation in limit calculation at the two sides of Eq. (36):

$$V_\infty(z) = \lim_{k\to\infty} V_k(z) = \lim_{k\to\infty} \frac{(Q + Q_1 z^{-1})H(z)U_k(z)}{1 - \beta[P - (Q + Q_1 z^{-1})H(z)]}. \tag{37}$$

If P and β all are 1, at the same time, the following inequality is satisfied by[18]

$$\left\|\beta P - \beta[Q + Q_1 z^{-1}]H(z)\right\|_\infty < 1. \tag{38}$$

Eq. (37) can be simplified by

$$V_\infty(z) = \lim_{k\to\infty} U_k(z) = U_d(z). \tag{39}$$

That is, the controller signal $u_k(z)$ is replaced by $\beta v_k(z)$ when infinite iteration is operated, and the error signal will become zero. According to Eqs. (35) and (39), the error signal can be shown as

$$\lim_{k\to\infty} E(z) = H(z)[\lim_{k\to\infty} U_k(z) - \beta \lim_{k\to\infty} V_k(z)] = H(z)[U_d(z) - \beta V_\infty(z)] = H(z)[U_d(z) - \beta U_d(z)] = 0 \tag{40}$$

The convergence of AILC has been demonstrated according to Eqs. (39) and (40), and a perfect controller signal u_d has been obtained as power amplifier input. Therefore, the AILC algorithm as the feed-forward compensation controller can be adopted in the application of AMB unbalance vibratory compensation.

According to the startup time and the variability of the rotor frequency from static suspension to one fixed speed, the equation of β is given as

$$\beta = \left(\frac{f}{f_d}\right)^n, \tag{41}$$

where f is the rotor frequency, f_d is a given frequency, the action of n is to reduce the value of β when f is far away from f_d, usually, n is greater than 2. In the startup process, due to $f \ll f_d$, the value of β should be very small, it can weaken the influence of V_k on the AMB generalized plant. However, β will be close to 1 if $f \approx f_d$, it can enhance the effect of repetitive learning and can make the error signal to converge toward zero.

4 Simulation of the Two Algorithms

In view of only having good learning performance for one fixed frequency of OILC and AILC algorithms, here, the compensatory frequency is supposed as f_d=200 Hz. Because A/D sampled frequency f_s=20 kHz, the range of n can be calculated by $n \in [0, 99]$ according to Eq. (24), that is, it has 100 memory points in one control period. Table 2 gives the weight coefficients of the learning laws of AILC and OILC in Eq. (25) and Eq. (26). The learning effects about both laws are displayed in Fig. 6.

Table 2. Weight coefficients of AILC and OILC

AILC			OILC	
P	Q	Q_1	P	Q
0.995	0.7	0.3	0.995	1.0

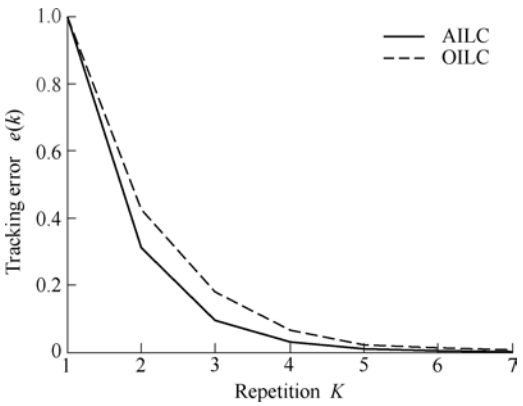

Fig. 6. Tracking abilities of AILC and OILC

Fig. 6 shows the asymptotic convergence about the two ILC algorithms, however, AILC has better convergent speed than OILC.

AILC and OILC algorithms are separately added into the Eq. (11) according to Eqs. (5), (25)–(27) to verify the advantage of AILC. The parameters of AMB system in Eq. (11) and PID controller are the same as them in Fig. 4. Here, the rotational frequency f is also assumed to be 200 Hz, and the eccentricity e is also 15 μm. Fig. 7 shows the rotor orbits and radial runout displacements with AILC compensation, and Fig. 8 shows the rotor trajectory with OILC compensation.

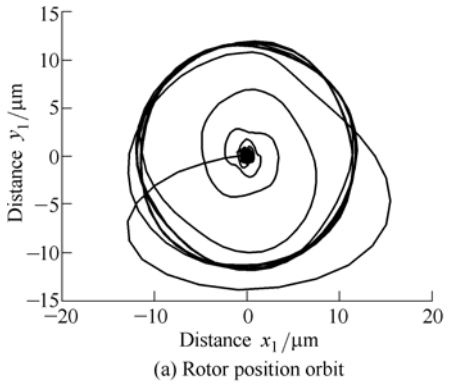

(a) Rotor position orbit

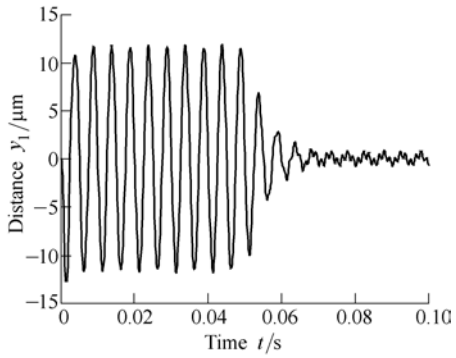

(b) Rotor runout in axis x_1

Fig. 7. Rotor trajectory with AILC compensation

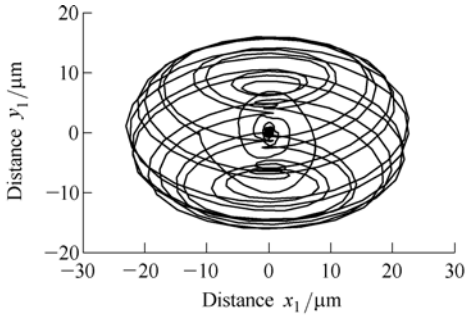

(a) Rotor position orbit

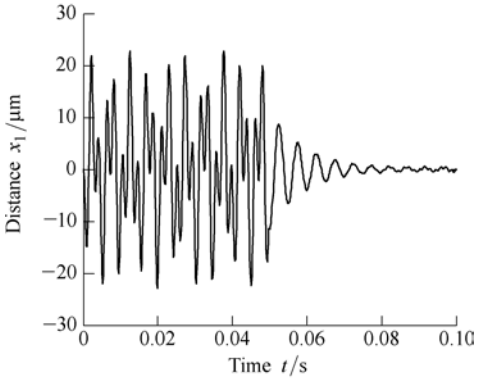

(b) Rotor runout in axis x_1

Fig. 8. Rotor trajectory with OILC compensation

In Fig. 7(a), the rotor has perfect rotary trajectory in the process of unbalance compensation of AMB system. While in Fig. 8 there is some interference, which may affect control system stability. And the convergent speed in Fig. 8(b) is slower than that in Fig. 7(b). From Fig. 7 and Fig. 8, the AILC algorithm has better compensation effects than OILC in the application of AMB unbalance vibratory displacement compensation.

5 Experiment Results

Fig. 9 shows the factual AMB system, which is accordant with the structure in Fig. 5. Rotor system, thrust magnetic bearings, radial magnetic bearings and power amplifier construct the generalized plant. Both PID control and AILC feed-forward compensation programs are implemented by PC, DSP2407A and PCI card. Furthermore, sensor drive can change displacement signals into voltage signals for processing, and the motor drives the rotor.

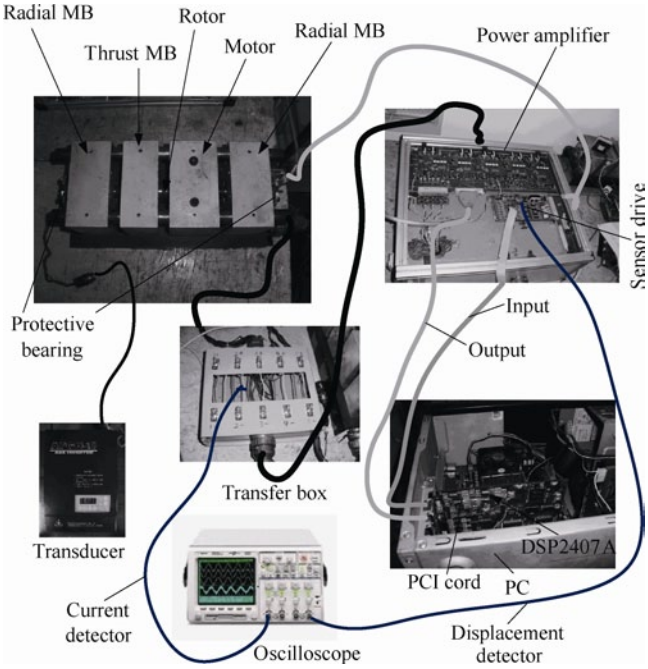

Fig. 9. Factual AMB operational system

The unbalance compensation is implemented at 200Hz, and some relevant coefficients of AILC are assigned as follows: f_d=200 Hz, Q=0.7, Q_1=0.3, and P=0.995. The rotational frequency f in Eq. (41) is computed by the CAP unit and the Periodic Interrupt of DSP through the pulse signal, and the signal comes from one small trough on rotor surface. The parameters of PID feedback controller are compatible with those adopted in the previous simulation. Fig. 10 shows the waveforms of rotor displacements and control currents in the experiment of AMB system with and without AILC at 200 Hz. In Fig. 10(a), the rotor radial displacement curve (v_1 in Fig. 1) with compensation becomes straightness compared to the displacement without compensation, while the amplitude of the control current with AILC is bigger than that without AILC in Fig. 10(b), it is conformable to the analysis in section 2.

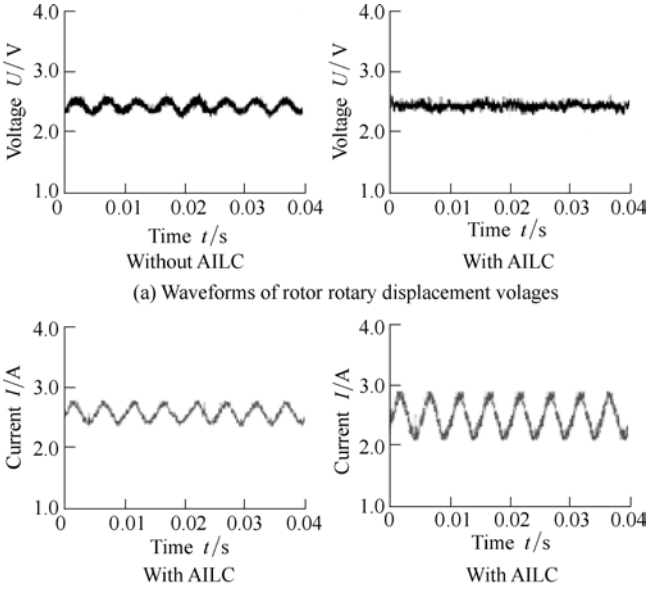

Fig. 10. Waveforms of displacements and control currents with and without compensation at 200 Hz

In other words, to enhance the active control effects and amplify the generalized dynamic stiffness, the control current should be increased. Fig. 11 gives the amplitude of the radial runout according to FFT and the relationship (v_1=20 000x_1) between displacement voltage v_1 and radial runout x_1, and Fig. 12 gives the FFT of currents. The two FFT are achieved through dealing with the data of those curves stored in oscilloscope. The relevant amplitudes are given in Table 3.

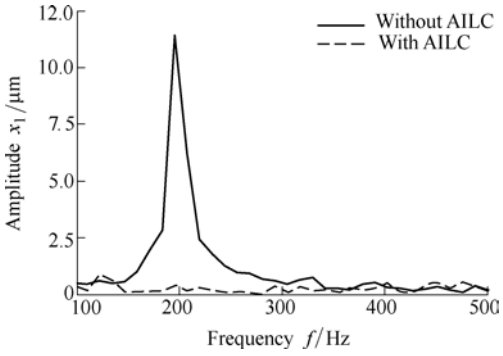

Fig. 11. Amplitude of radial runout at 200 Hz

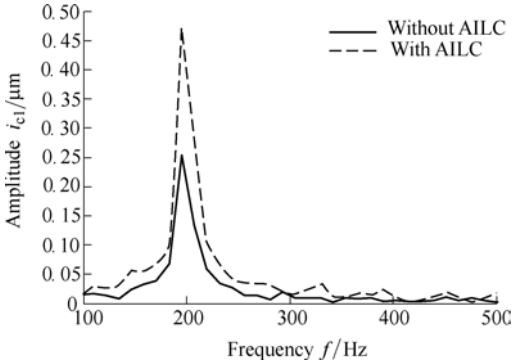

Fig. 12. Amplitude of control current at 100 Hz

Table 3. Values of displacement and current amplitudes with and without AILC

Without AILC		With AILC	
Displacement x_1/μm	Current i_{c1}/A	Displacement x_1/μm	Current i_{c1}/A
11.5	0.25	1.0	0.47

From Fig. 11, Fig. 12, and Table 3, the amplitude of radial runout is reduced from 11.5 μm to 1.0 μm after using AILC, while the amplitude of compensated current is 0.22 A bigger than that of the original current without AILC compensation. The above results prove that the radial displacement fluctuations of the system with feed-forward compensation are obviously reduced. The reduction of displacement can improve the rotor rotating precision, and reduce machining error effectively in an AMB rotating tool.

6 Conclusions

(1) The rotor radial runout orbits are achieved through solving those mechanical matrix equations. As the runout is undesirable in application, the AILC method is proposed to compensate the unbalance effects of rotor runout.

(2) AILC algorithm can adaptively and iteratively learn frequency-variable rotor radial displacement signals and implement well compensation at one fixed rotary frequency.

(3) AILC algorithm can significantly reduce the rotor runout and has a better robustness compared to OILC for variable rotor speed. Furthermore, AILC can provide probability for variable speed unbalance compensation.

References

[1] SCHWEITZER G, TRAXLER A, BLEULER H. *Magnetic bearings: theory, design, and application to rotating machinery*[M]. Berlin: Springer, 2009.

[2] JING Minqing, LI Zixin, LUO Min, et al. Unbalance response and touch-rubbing threshold speed of rotor subjected to nonlinear magnetic forces[J]. *Chinese Journal of Mechanical Engineering*, 2008, 21(2): 1–4.

[3] HU Yefa, GAO Xiaoming, WU Huachun. The study of unbalance compensation for the rotor of magnetic bearings[J]. *Machinery*, 2006, 44(504): 24–26. (in Chinese)

[4] TAGUCHI N, ISHIMATSU T, WOO S J, et al. Unbalance compensation of magnetic bearings[C]//*20th International Conference on Industrial Electronics, Control and Instrumentation*, *Industrial*, Bologna, Italy, September 5–9, 1994: 2 051–2 056.

[5] LUM K Y, COPPOLA V T, BERNSTEIN D S. Adaptive autocentering control for an active magnetic bearing supporting a rotor with unknown mass imbalance[J]. *IEEE Transactions on Control Systems Technology*, 1996, 4(5): 587–597.

[6] MIZUNO T. An unified approach to controls for unbalanced compensation in active magnetic bearings[C]//*Proceedings of the 1998 IEEE International Conference on Control Applications*, Trieste, Italy, September 1–4, 1998: 1 063–1 067.

[7] NONAMI, LIU Zihe. Adaptive unbalance vibration control of magnetic bearing system using frequency estimation for multiple periodic disturbances with noise. *Proceedings of the 1999 IEEE International Conference on Control Applications*, Kohala Coast, HI, USA, August 22–27, 1999: 576–581.

[8] ARIAS M M, SILVA N G. Finite element modeling and unbalance compensation for a two disks asymmetrical rotor system[C]//*5th International Conference on Electrical Engineering, Computing Science and Automatic Control*, Mexico City, Mexico, November 12–14, 2008: 386–391.

[9] JASTRZEBSKI R P, POLLANEN R. Compensation of nonlinearities in active magnetic bearings with variable force bias for zero and reduced-bias operation[J]. *Mechatronics*, 2009, 19(5): 629–638.

[10] INOUE T, LIU Jun, ISHIDA Y, et al. Vibration control and unbalance estimation of a nonlinear rotor system using disturbance observer[J]. *Journal of Vibration and Acoustics*, 2009, 131(3): 1–8.

[11] COSTIC B T, QUEIROZ M S, DAWSON D N. A new learning control approach to the active magnetic bearing benchmark system[C]//*Proceedings of 2000 American Control Conference*, Chicago, IL, USA, June 28–30, 2000: 2 639–2 643.

[12] CHIARINI H G, MANDOLESI P S. Unbalance compensation for active magnetic bearings using ILC[C]//*Proceedings of the 2001 IEEE International Conference on Control Applications*, Mexico City, Mexico, September 5–7, 2001: 58–63.

[13] BI Chao, WU Dezheng, JIANG Quan, et al. Automatic learning control for unbalance compensation in active magnetic bearings[J]. *IEEE Transactions on Magnetics*, 2005, 41(7): 2 270–2 280.

[14] GU Jialiu. *Rotor dynamic*[M]. Beijing: National Defense Industry Press, 1985.

[15] KOSAKIi T, SANO M, TANAKA K. Model-based fuzzy control system design for magnetic bearings[C]//*Proceedings of the Sixth IEEE International Conference on Fuzzy Systems*, Barcelona, Spain, July 1–5, 1997: 895–899.

[16] SUN Yanhua, HO Y S, YU Lie. Dynamic stiffnesses of active magnetic thrust bearing including eddy-current effects[J]. *IEEE Transactions on Magnetics*, 2009, 45(1): 139–149.

[17] HU Yefa. *Magnetic bearings basic theory and application*[M]. Beijing: China Machine Press, 2006.

[18] JUNG H M, TAE Y D, MYUNG J C. An iterative learning controls scheme for manipulators[C]//*Proceedings of the 1997 IEEE/RSJ International Conference on Intelligent Robot and Systems*, Grenoble, France, September 7–11, 1997: 759–765.

[19] BRIAN E, LEE H C, DOUGLAS A, et al. Combined H∞-feedback control and iterative learning control design with application to nanopositioning systems[J]. *IEEE Transactions on Control System Technical*, 2010, 18(2): 336–351.

[20] AHN H S, CHEN Y Q. Periodic adaptive learning compensation of state-dependent disturbance[J]. *IET Control Theory Application*, 2010, 4(4): 529–538.

Biographical notes

GAO Hui, born in 1981, is currently a PhD candidate at *College of Mechanical and Electrical Engineering, Nanjing University of Aeronautics and Astronautics, China*. His research interest is vibration compensation control of AMB system when the rotor high-speed rotating.
Tel: +86-13813925147; E-mail: gaohui2010@nuaa.edu.cn

XU Longxiang, born in 1959, is currently a professor at *College of Mechanical and Electrical Engineering, Nanjing University of Aeronautics and Astronautics, China*.
E-mail: fqp@nuaa.edu.cn

ZHU Yili, born in 1987, is currently a PhD candidate at *College of Mechanical and Electrical Engineering, Nanjing University of Aeronautics and Astronautics, China*. His research interest is vibration compensation control of AMB system when the rotor high-speed rotating. His research interest is dynamics.
E-mail: nuaazyl@nuaa.edu.cn